

Self-Sustained Collective Oscillation Generated in an Array of Non-Oscillatory Cells

Yue Ma* and Kenichi Yoshikawa†

*Spatio-Temporal Order Project, ICORP, Japan Science and Technology Agency (JST) &
Department of Physics, Graduate School of Science, Kyoto University, 606-8502, Japan*

(Dated: June 21, 2024)

Oscillations are ubiquitous phenomena in biological systems. Conventional models of biological periodic oscillations usually invoke interconnecting transcriptional feedback loops. Some specific proteins function as transcription factors, which in turn negatively regulate the expression of the genes that encode these “clock proteins”. These loops may lead to rhythmic changes in gene expression in a cell. In the case of multi-cellular tissue, collective oscillation is often due to synchronization of these cells, which manifest themselves as autonomous oscillators. In contrast, we propose here a different scenario for the occurrence of collective oscillation in a group of *non-oscillatory* cells. Neither periodic external stimulation nor pacemaker cells with intrinsically oscillator are included in present system. We observe and analyze a coupling-induced oscillation, inherent to the phenomenon of wave propagation due to intracellular communication.

PACS numbers: A PACS will be appear here

I. INTRODUCTION

Oscillation is ubiquitous in nature, not only in physics and chemistry but also biology. Biological oscillations can be observed over a wide range of time- and population-scales, from a circadian rhythm of about 24 hours [1] to a segmentation clock of less than 2 hours [2], from whole-body oscillatory fevers [3] to periodic protein production in a single cell [4]. There are also many theoretical models to explain these phenomena. Despite their diversity of biological insights, these models share some common points.

Proteins are produced by the transcription and translation of specific sequences of DNA. On the other hand, proteins can bind to a transcription promotor on DNA and hence suppress or enhance gene expression. A transcriptional negative feedback loop [5, 6] and a delay [7, 8] in the inner cellular gene-protein network are considered to be important elements that contribute to the oscillatory expression of DNA and protein production. From the perspectives of dynamical systems, such oscillations are limit cycles that can be generated from Hopf bifurcation by choosing an appropriate parameter set. Consequently, in the case of a cell group or multi-cellular organism with an oscillatory character, such as cardiac tissue and a segmentation clock in the tail of PSM (Presomitic Mesoderm), the synchronization of coupled oscillators is often used to explain the observed collective oscillation [9, 10, 11].

However, periodic oscillation is only a small part of the dynamical behavior of a cell. Oscillation may cease if the conditions are changed, and most cells tend to settle into a seeming stable state. For example, electrical activity in β -cells exhibits slow periodic oscillation at the macro

scale of islets of Langerhans, while much faster excitability instead of oscillation when isolated [12, 13]. Another example of biological oscillation is well-studied circadian clock. Most recent studies have suggested that negative transcriptional feedback is not sufficient, and in some cases not even necessary, for circadian oscillation. Instead, intracellular signaling, such as that involving Ca^{2+} and cAMP, together with transcriptional feedback plays a key role in long-term circadian pacemaking [14]. This raises the possibility that intrinsic oscillatory cells are not indispensable in an oscillatory organism. In this paper, we propose a novel mechanism for oscillation to take place in a group of cells with coupling. In contrast to the conventional mechanism of synchronized oscillators, none of the individual cells in our model is intrinsically oscillatory. Instead, collective oscillation is due to intracellular coupling and wave propagation.

We consider that cells are excitable and can be described by FitzHugh-Nagumo (FHN) equations. The coupled FHN model is a well-studied paradigm for an excitable medium in the context of chemical oscillators, computational neuroscience, and so on. An oscillating pattern can usually be obtained by setting the parameters beyond a Hopf bifurcation. In this paper, however, we focus our attention on another possible scenario, i.e., occurrence of collective oscillation from non-oscillatory system. To induce oscillation into a non-oscillatory system, researchers proposed several approaches, for example, applying a periodic stimulation [15], coupling the system with an oscillatory boundary [16], introducing heterogeneity into excitable media [17]. A commonly used idea is to push a subthreshold quiescent element over into the oscillatory regime by extra force or coupling, and generate pacemaker cells. However, little attention has been paid to the emergence of oscillation in systems that are completely independent of oscillating elements. Unlike previous studies, there are two “engines” in our model to drive the self-sustained collective oscillation, neither of which is oscillatory pacemaker. The one is bistable cell

*Electronic address: dr.mayue@gmail.com; Corresponding author

†Electronic address: yoshikaw@scphys.kyoto-u.ac.jp

switching between two stable states, the other is mono-stable cell with excitability. Two engines work cooperatively due to the wave propagation.

A few studies in the context of mathematics and physics have revealed the possibility of collective oscillating patterns. The first example was proposed by Smale [18], who found that two “dead” cells can become “alive” via diffusive coupling. More recently, other studies have examined this behavior in detail [19, 20]. In-phase and anti-phase self-sustained oscillation of excitable membrane via bulk coupling have been observed [21]. The models considered in these reports have mostly involved coupled identical excitable cells with mono-stability. On the other hand, in a bistable system, a stationary front can bifurcate into a pair of fronts that propagate in opposite directions, which is known as nonequilibrium Ising-Bloch (NIB) bifurcation [22, 23]. Perturbation for the occurrence of NIB bifurcation can be induced by local spatial inhomogeneity [24]. A more global analysis showed that the NIB point is only part of the story, and concluded that an unstable wave front is intrinsic to media that are spatially inhomogeneous [25, 26]. An unstable wave front may manifest itself as a reflected front, tango wave [27], pacemaker [28] and so on. In this paper, we present new ways to think about these phenomena beyond mathematics and physics, and extend their application to biological oscillators.

Moreover, although most studies have been performed on a spatial continuum described by partial differential equations (PDE), continuum models neglect the effects of cellular discreteness [29]. In fact, from the viewpoint of biology, the size of cells can not be decreased infinitely. This intrinsic property is difficult to ignore, especially at the stage of initial development of an organism, when the cell size is comparable to that of tissue. In addition, there are mathematical reasons to explore the system dynamics with spatial discretization. PDE and ODE (ordinary differential equations) have different theoretical frameworks and produce different results. Several significant features of discreteness, such as *wave propagation failure* [30], can not occur in a continuum model. Therefore, in this paper we will consider an array of spatially discrete cells, and discuss the impact of discreteness.

II. DESCRIPTION OF THE MODEL

A. One-dimensional cellular array

In this paper, we consider cells in one-dimensional space. Cells are coupled by intracellular signaling molecules, which flow through channels in a membrane due to concentration difference or depolarization-mediated flux. An intracellular small-molecule signal then integrates with transcriptional feedback loops of adjacent cells. We assume that this coupling signal is regulated by the expression of an activator u and interacts

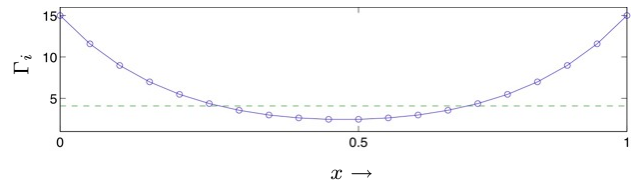


FIG. 1: Profile of Γ_i obtained from Eq.(4), when $\Gamma_0 = 15, \xi = 5$.

with neighboring cells in a diffusion-like manner. If we include an inhibitor, a one-dimensional array of N cells can be described as

$$\dot{u}_i = f(u_i, v_i, \Gamma_i) + \tilde{D}(u_{i-1} + u_{i+1} - 2u_i) \quad (1)$$

$$\dot{v}_i = g(u_i, v_i) \quad (2)$$

where $i \in \{1 \dots N\}$ is the index of the cell in the chain and \tilde{D} is the coupling strength of u . f and g are reaction functions of the activator and inhibitor, respectively. The boundary condition is zero flux, i.e., $u_0 = u_1$ and $u_N = u_{N+1}$. Γ_i is an environmental parameter, which will be discussed in detail later.

In this study, we only consider coupling of the activator. For most of the models that have been used to study pattern formation, diffusion is assumed to occur for every element. Specially, much greater diffusion of the inhibitor is necessary to induce Turing instability [31]. However, a cell's membrane is very selective for passage of substances. Complicated intracellular reactions usually take place locally, but are triggered by only one or a few specific signaling molecules. For example, while the segmentation clock involves the cyclic expression of many genes, the crucial pathway for coupling only involves the transmembrane receptor Notch1 [32]. Thus, in the context of biology, we only consider coupling with the activator, and the inhibitor in our model is merely a local state variable.

B. Active factor

The development of a multicellular organism begins with a single cell, which divides and gives rise to cells with different typologies. Different cells are organized according to certain secreted chemicals, called morphogens. Despite improvements in experimental and theoretical approaches, the mechanisms of morphogenesis are still unclear. Usually, morphogens are considered to be produced at specific sites and diffuse through the organism [33]. Quite recently, evidence of a “shuttling-based” mechanism has been presented [34]. The key in such models is their ability to define a robust and scaling profile, usually a concentration gradient, of morphogens. More broadly, we can suppose that some environmental parameters act as morphogens. The environment in which an organism develops supplies nutrition for growth, and the intracellular volume in direct contact with the border gets more and that deep inside cells gets less.

In this paper, we do not consider any specific chemical substance, and instead merely suppose that there is a certain factor, which we refer to as the active factor, to obtain information regarding the relation between position and cell dynamics.

Without losing generality, we assume that the active factor Γ is constant at the boundaries of an organism. It diffuses into the organism field with a diffusion constant D_a , and is degraded at rate α . Thus, we have

$$\frac{\partial \Gamma}{\partial t} = D_a \frac{\partial^2 \Gamma}{\partial x^2} - \alpha \Gamma. \quad (3)$$

Since our model is based on coupled ODEs independent of spatial variation, the profile of the active factor satisfies a scaling property. By normalizing the field size to one, we can get a steady profile ($\partial \Gamma / \partial t = 0$) of Γ as

$$\Gamma(x) = \frac{\Gamma_0}{e^{-\xi} - e^{\xi}} ((e^{-\xi} - 1)e^{\xi x} - (e^{\xi} - 1)e^{-\xi x}), \quad (4)$$

where $\Gamma_0 = \Gamma(0) = \Gamma(1)$ is the value at two boundaries, and $\xi = 1/\lambda = \sqrt{\alpha/D_a}$ is the inverse of the decay length. A typical profile of $\Gamma(x)$ is shown in Fig. 1. Blue circles indicate the value of Γ for discrete cells ($N = 20$ in the figure) placed uniformly in the scaling field.

C. Bistability

The above-mentioned active factors can affect the fate of cells in a concentration dependent manner [35]. We assume that cells normally prefer to live in a stable state, and a high concentration of active factor can excite cells into another stable state. This kind of bistability is very important and has been observed in various biological systems, such as cell signaling and neural processes [36, 37, 38]. Moreover, it was recently suggested that stochastic fluctuation plays an important role in the nature of the transition between bistable states [39].

Usually, bistability arises from positive genetic regulation loops [37, 40, 41]. Conventional biochemical theory has clarified the key-lock relationship between a transcription factor and promoter. In this paper, however, we shed light on the physical regulation of protein production, which has been much less considered by biochemists. We consider the origin of the bistability based on the intrinsic property of DNA molecule. A DNA molecule that is longer than several micrometers (over 100 000 base pairs) shows the characteristics of a semi-flexible polymer, which exhibits a discrete transition between coiled and compact states; i.e., a first-order phase transition for a single giant DNA molecule. This discrete transaction leads to the ON/OFF switching of DNA transcription, and hence the production of a specific protein [42]. In this transition process, the specific key-lock interaction has little influence on the global region of DNA, and instead the robust transition on the region with the order of several hundreds base-pairs is induced by “nonspecific”, abundant chemical species such

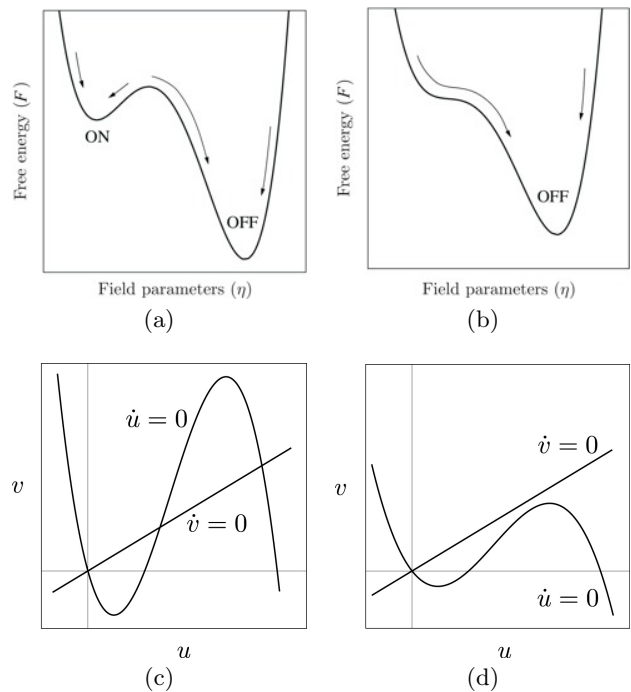


FIG. 2: Free energy (a & b) and nullcline diagrams (c & d) in bistability (a & c) and mono-stability (b & d), respectively.

as the concentrations of polyamine, mRNA, ATP, and so forth [42, 43, 44]. Moreover, RNA [45], protein [46] and other molecules [47] have also been shown to exhibit discrete switch between folding and unfolding or between active and inactive state. Although the details of the mechanism have not yet to be clarified, it is believed to play an important role in the self-regulation of gene expression in living cells, and might be a more universal law of morphogenesis than other biochemical reactions.

The ON/OFF switching character of a DNA molecule is the manifest of double minimum free energy profile with respect to the parameter describing the high-order structure of DNA. Without losing generality, we assume the kinetic is quartic, as shown in Fig. 2(a), with respect to specific a “field parameter” or an order parameter η , such as density. Usually, it stays in either the OFF or ON state corresponding to the intracellular concentrations of abundant nonspecific chemical species, such as ATP, polyamines, small ions, etc. Consequently, the state of DNA’s higher order structure, either coiled or compact, affects the process of transcription. At a molecular scale, since the effect of inertia can be ignored compared to that of viscosity, the change in density is in proportion to generalized force, so we have $\partial \eta / \partial t \sim -\partial F / \partial \eta$. Clearly, due to the assumption of a quartic kinetic of F , $-\partial F / \partial \eta$ is a cubic function. Based on these considerations, we choose a reaction function for a single cell in the form of FitzHugh-Nagumo (FHN) equations. Moreover, we can identify an active factor as a certain signaling protein, such as ComK in soil bacterium to develop a “competence” event [39], or chemicals in the intracellular envi-

ronment, such as mRNA, ATP, etc. [42, 43, 44]. We suppose that cells with a high concentration of active factor are capable of switching between OFF and ON states (bistability), as shown in Fig. 2(a), while cells with a low concentration can only exhibit the OFF state, as shown in Fig. 2(b).

If we include an inhibitor, the dynamical reaction function of each cell can be described as

$$\dot{u} = f(u, v, \Gamma) = \Gamma u(u - \alpha)(1 - u) - v \quad (5)$$

$$\dot{v} = g(u, v) = \epsilon(\beta u - v) \quad (6)$$

where u is a variable related to the activity of DNA and v is the inhibitor that changes slowly compared to u in the case of $\epsilon \ll 1$. Note that the kinetics of inhibitor here is a rather natural unit process in many of biochemical reactions. Throughout this paper, the following parameters are fixed

$$\alpha = 0.3, \beta = 0.5, \epsilon = 0.02. \quad (7)$$

Figures 2(c)&(d) show the nullclines with bistability and mono-stability for when Γ is large and small, respectively. Specifically, with the above parameters, the critical value of Γ , which separates the two kinds of stability, is 4.08. Thus, in the case of the spatial profile of Γ_i as shown in Fig. 1, only the 8 central cells (7^{th} - 14^{th}) are mono-stable, while the others are bistable. Again, none of the cells show oscillation in the absence of coupling.

If we substitute Eq. (5&6) into Eq. (1&2), we get the system equations used in this paper.

$$\dot{u}_i = \Gamma_i u_i(u_i - \alpha)(1 - u_i) - v_i \quad (8)$$

$$+ \tilde{D}(u_{i-1} + u_{i+1} - 2u_i) \quad (9)$$

$$\dot{v}_i = \epsilon(\beta u_i - v_i)$$

When we change the coupling strength \tilde{D} , we observe the occurrence, variation and disappearance of self-sustained collective oscillation in the cell array.

III. SELF-SUSTAINED COLLECTIVE OSCILLATION

A. Normal collective oscillation

Figure 3(a) shows a typical oscillation when the coupling strength $\tilde{D} = 0.7$. Figure 4(a) shows an enlarged view of a single period of oscillation. As the initial condition, we set the 1st cell as being excited, since stimulation is usually input from the border. Initially, ($0 < t \lesssim 80$), a traveling wave appears due to excitation at the border. The traveling front then sweeps over the cell array and makes all of the cells excited (see Fig. 4(b)). Although the central cells are also turned ON due to the interaction with other cells, they can not stay in the excitable state for a long time. Instead, they soon return to their stable equilibrium (see Fig. 4(c)), and hence generate two

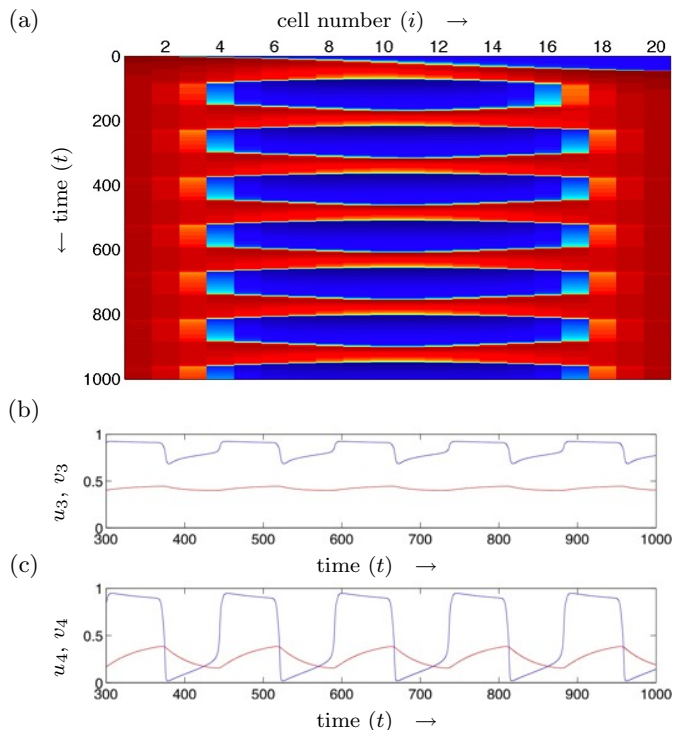


FIG. 3: Collective oscillation observed in a chain of cells when $\tilde{D} = 0.7$ in Eqs. (8& 9). (a) Spatio-temporal plot of the collective oscillation of u_i . The colors red and blue indicate $u_i = 1$ and $u_i = 0$, respectively. (b, c) Waveforms of u (blue) and v (red) in the 3rd and 4th cells.

counterpropagating wave backs, as shown in Fig. 4(d). These two wave backs propagate outward until the 3^{rd} and 18^{th} cells and stop suddenly due to the spatial discreteness (see Fig. 4(e)). The “wall” cells do not jump from the ON state to the OFF state and only exhibit slight oscillation closed to their equilibrium. As an example, the difference between the 3^{rd} and 4^{th} cells is shown in Fig. 3(b, c). At this critical interface, the inhibitor v slowly decreases so that the 4^{th} and 17^{th} cells restore excitability after a while. The central cells can then be excited again by the pair of reflecting wave fronts, as shown in Fig. 4(f). Pushed by the wave, the central cells will be excited again. This process repeats and causes the collective oscillation inside multi-cell tissue without oscillatory cells.

B. Stationary state before birth of oscillation

The above collective oscillation can be observed when the coupling strength is larger than a threshold, below which wave backs (see Fig. 4(d)) fail to reflect, and the state in Fig. 4(e) is maintained. Figure 5 shows a spatio-temporal diagram, where the central cells stay silent while excited bands appear close to the two borders.

Note that this phenomenon could not take place in a continuum counterpart. The existence of a coupling

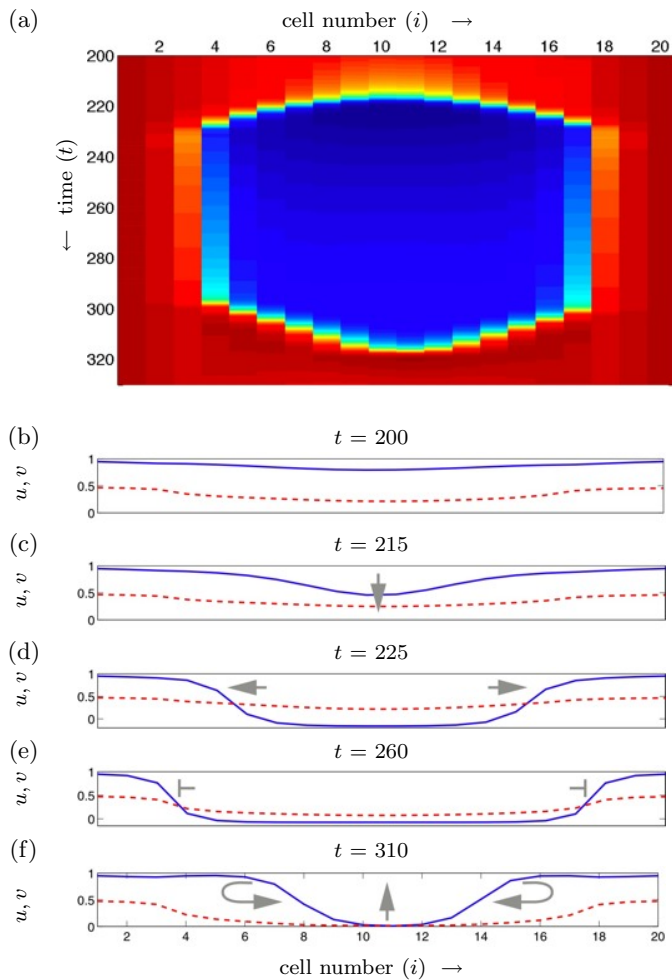


FIG. 4: (a) Spatio-temporal diagram of u_i over a single period, (b)-(f) Snapshots of u and v at several time points in one period. This illustrates the change in wave propagation at different stages. Blue solid curves and red dashed curves indicate u and v , respectively.

strength threshold under which *wave propagation failure* occurs is unique to a spatially discrete system. In addition, there is another threshold, which is even smaller, for which the *wave front* stops propagating. In this case, the excited signal at the border fails to propagate forward, but we would like to postpone this interesting phenomenon on another paper, since it is less related to present work.

C. In-phase and anti-phase period doubling oscillation closed to the boundary

With an increase in the coupling strength \tilde{D} , the characteristics of oscillation can be changed. Figure 6 shows that the position of oscillation periodically shifts. The 3rd and 18th cells oscillate with a nearly doubled period, in anti-phase (Fig. 6(b,c)). Globally, tissue oscillates in two groups with the same cell populations but different

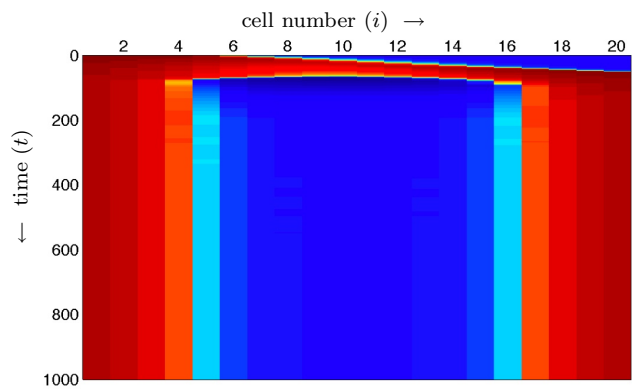


FIG. 5: Spatio-temporal diagram of u_i in a stationary state. Wave propagation stops and no oscillation occurs in the case of weak coupling $\tilde{D} = 0.47$.

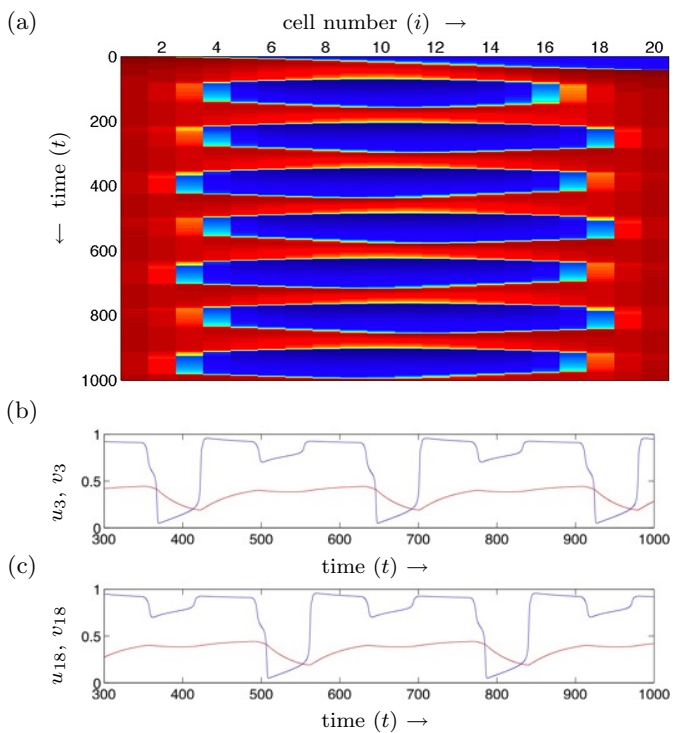


FIG. 6: Anti-phase mode in period doubling produces collective oscillation with a periodic position shift when $\tilde{D} = 0.8$. (a) Spatio-temporal diagram of u_i . The colors red and blue indicate $u_i = 1$ and $u_i = 0$, respectively. (b) and (c) are waveform diagrams of the 3rd and 18th cells. Activator u and inhibitor v are shown in blue and red, respectively.

positions: No. 3-No. 17 (15 cells) and No. 4-No. 18 (15 cells), respectively.

Interestingly, by slightly increasing the coupling strength \tilde{D} , say to $\tilde{D} = 0.9$, we found a different type of period doubling, as shown in Fig. 7. For comparison with the case of $\tilde{D} = 0.8$, although the critical interface between ON and OFF shifts periodically as in Fig. 6,

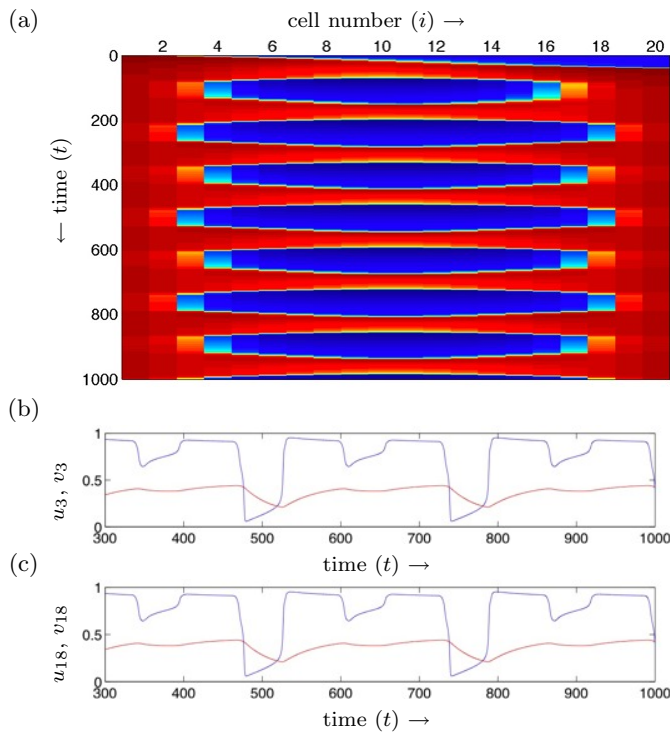


FIG. 7: In-phase mode in period doubling produces collective oscillation with a change in the periodic population when $\tilde{D} = 0.9$. (a) Spatio-temporal diagram of u_i . The colors red and blue indicate $u_i = 1$ and $u_i = 0$, respectively. (b) and (c) are waveform diagrams of the 3rd and 18th cells. Activator u and inhibitor v are shown in blue and red, respectively.

there is no phase difference between the 3rd and 18th cells. As is clearly shown in their waveform (Fig. 7(b,c)), these two boundary cells oscillate in-phase, instead of anti-phase (Fig. 6(b,c)). Therefore, in the present condition, a periodic change does not take place in the position of oscillation. Instead, the population of oscillating cells changes. More precisely, tissue oscillates in two groups: No. 3-No. 18 (16 cells) and No. 4-No. 17 (14 cells), respectively.

Moreover, by setting the initial condition of the cells identically, i.e., all in the ON state at $t = 0$, we found checked that same symmetric collective oscillation can also occur in the case of $\tilde{D} = 0.8$. Therefore, we conclude that these two types of oscillation are caused by the same bifurcation. Because the wavefront propagates faster with larger \tilde{D} , a larger coupling strength can reduce the time lag between the two boundary cells being stimulated. If the time lag is smaller, the two boundaries converge to in-phase oscillation. On the other hand, if the time lag is large, they will exhibit anti-phase oscillation.

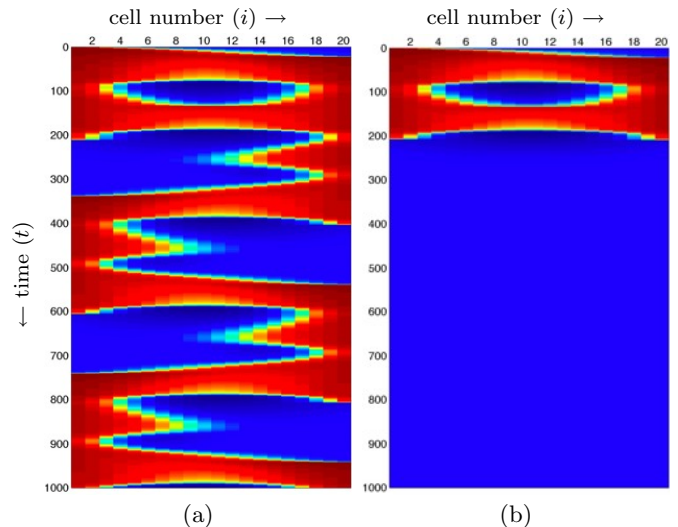


FIG. 8: Spatio-temporal diagram of u_i . Red and blue indicate $u_i = 1$ and $u_i = 0$, respectively. (a) $\tilde{D} = 2.53$, oscillation starts to collapse; (b) $\tilde{D} = 2.6$, oscillation ceases after one cycle.

D. Oscillation death

With a increase in coupling strength \tilde{D} , we observed that the change in the periodic position or population stopped, and normal oscillation returned. In comparison to the case of $\tilde{D} = 0.7$, the total population of oscillating cells increased from 14 (No. 4 to No. 17) to 16 (No. 3 to No. 18).

The oscillation suddenly dies when \tilde{D} is as large as 2.6. Figure 8(b) clearly shows that the central cells start to oscillate after all of the cells are excited, but this oscillation is not sustained. In this strong coupling condition, the boundary cells can not recover their excitability, so that the wave front propagating from the center is unable to stop and reflect to generate successive oscillation.

Before the oscillation stops, there is a narrow parameter region of $2.53 \leq \tilde{D} \leq 2.56$, where only one side of the “wall” alternatively collapses, and a complicated period-4 collective oscillation is observed (Fig. 8(a)).

E. Overall perspective

Here, we sweep the coupling strength \tilde{D} from 0.45 to 2.7, and summarize the variation in the oscillation period and position of the left border of oscillation region. Figure 9(a) shows a diagram of the cell number for the left boundary of collective oscillation. If the coupling strength is smaller than 0.48, there is no oscillation, and 4 cells from the tissue border are excited while cells 5–16 are silent. Oscillation takes place when the wave back passes the 4th cell at $\tilde{D} = 0.48$. The border then shifts between 3 and 4, while in-phase and anti-phase period doubled oscillation occur, between $0.78 < \tilde{D} < 0.97$. Fi-

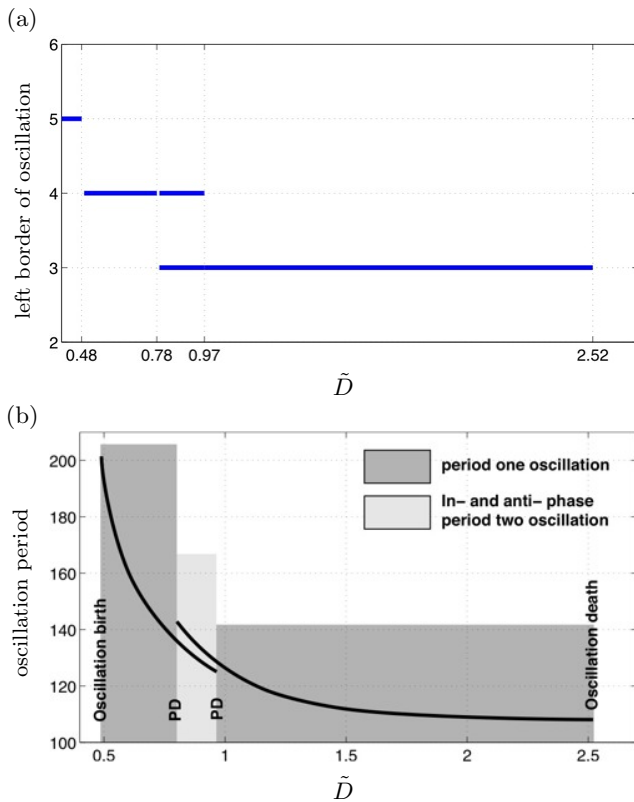


FIG. 9: Phase diagram of (a) the position (cell index) of the left border of oscillation (b) the oscillation period, with a change in the strength of coupling.

nally, the oscillation reaches a maximum region: from cells 3 to 18, until \tilde{D} is too large for oscillation to occur.

Variations in the period of oscillation are shown in Fig. 9(b). Once the central cells start to collectively oscillate, the period rapidly decreases when the coupling strength increases. The rate of the period decrease gradually slows. The period changes little in the region where \tilde{D} is large. This phenomenon occurs because the stationary interval (Fig. 4(e)) greatly contributes to the period of oscillation. The decrease in the stationary interval significantly shortens the period of oscillation when \tilde{D} is small. However, when \tilde{D} is large enough, the wave backs reflect immediately without stopping, and the period is determined mainly by the velocity of propagation.

There is a parameter region (light gray between PD in Fig. 9(b)) in which system manifests itself as period two oscillation with in-phase or anti-phase character (initial condition dependent). Although we denote the critical parameter value as PD, it is not a Period-Doubling bifurcation in traditional sense, which generates a pattern of alternately shorter and longer periodic. We will do more detailed investigation on this kind of spatio-temporal bifurcation phenomenon in our future work.

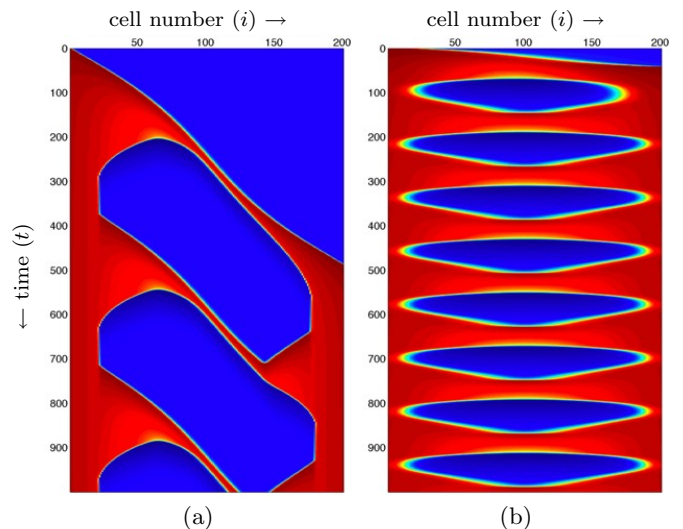


FIG. 10: Spatio-temporal diagram of u_i . Red and blue indicate $u_i = 1$ and $u_i = 0$, respectively. $N = 200$. (a) For cells growing in an open field, $\tilde{D} = D/\Delta x^2 = 0.7$. (b) For cells growing in a limited field, $\tilde{D} = D/\Delta x^2 = 70$.

IV. DISCUSSION

A. Discreteness vs. continuum

The above phenomena are generated in a spatially discrete system. As briefly introduced in Sec I, this discreteness is important in both a mathematical and biological sense. Let us discuss this significance in greater detail.

The diffusion term $D(\partial^2 u/\partial x^2)$ in a one-dimensional spatially continuous reaction-diffusion model can be formulated as $D(u_{i-1} + u_{i+1} - 2u_i)/\Delta x^2$ in its difference version. This type of conversion is a common approach to solving PDE numerically. The diffusion rate D usually does not change much for a specific substance under constant conditions. However, the coupling strength \tilde{D} we used in previous sections tends to be affected by various molecular biological factors. Here, we assume that the coupling is mainly due to the diffusion-like effects of substances, and \tilde{D} is approximately equal to $D/\Delta x^2$. Since the profile of the active factor has a scaling property, it is reasonable to suppose that this gradient works for a field of any size. Thus, we can study how a change in the field affects global dynamics.

During the initial period of development, cells have enough space for the population to increase. Thus, the distance between cells Δx is so great that \tilde{D} can be a relatively small value. Therefore, at the beginning, a group of cells may not exhibit oscillation, but are divided into several functional “layers”, as shown in Fig. 5. As cell division proceeds and the population grows, cells may become compacted. This decrease in Δx results in a greater coupling strength \tilde{D} , and collective oscillation may start to take place.

If the field in which cells continue to grow is open or

large enough, Δx and \tilde{D} will not change significantly. Figure 10(a) shows spatio-temporal diagrams with a 10-fold increase in the number of cells, $N = 200$. Other parameters are the same as those in Fig. 3. Obviously, more time is required for a wave to sweep over the organism. The period of oscillation and the phase difference between the two sides increase greatly.

On the other hand, if the cell population increases in a limited space, the distance Δx between cells becomes smaller and smaller, and the system manifests itself more like a continuum than a discrete system. In this case, the coupling strength will increase dramatically as a square with respect to the decrease in Δx . If the field is just filled when $N = 20$, then a 10-fold increase in N will result in a 100-fold increase in \tilde{D} . Thus, if $N = 200$, \tilde{D} is as large as 70. Under this condition, we have the spatio-temporal diagram given in Fig. 10(b). When we compare this with Fig. 3, there is little change in the period of collective oscillation. This suggests that the clock runs punctually when the size of organism does not grow.

In a mathematical sense, when the population of cells is large enough in a fixed field, the behavior of the organism will follow the solution of a specific partial differential equation, which is independent of the number of cells.

Moreover, during one period in Fig. 10(b), there is no sudden stopping of the wave front and a stationary interval as Fig. 4(a). Thus, the period of oscillation can be evaluated mainly in terms of the speed of wave propagation in the limited-field case and the duration of stationary interval in the open-field case.

B. Understanding the mechanism

Self-sustained collective oscillation is caused by the excitability of cells and their mutual interaction. The system involves complicated bifurcations. We present here some qualitative ideas regarding how this oscillation takes place.

From dynamical equations (5,6) and their nullcline shown in Fig. 2(c,d), we know that a single cell can exhibit either bistability or mono-stability. However, if we introduce coupling, the nullcline of one cell will dynamically change according to its own state and those of its neighbors. Because it was assumed that the communication between cells is only mediated via the activator u , the strict nullcline $\dot{v}_i = 0$ is independent of coupling.

$$v_i = G(u_i) = \beta u_i. \quad (10)$$

From Eqs.(1&5), we obtain the function for the nullcline $\dot{u}_i = 0$ as

$$v_i = F(u_i, \Gamma_i) = \Gamma_i u_i (u_i - \alpha)(1 - u_i) + \Delta U_i, \quad (11)$$

where $\Delta U_i = \tilde{D}(u_{i+1} + u_{i-1} - 2u_i)$ is the offset of the cubic function due to coupling. Thus, the nullcline $v =$

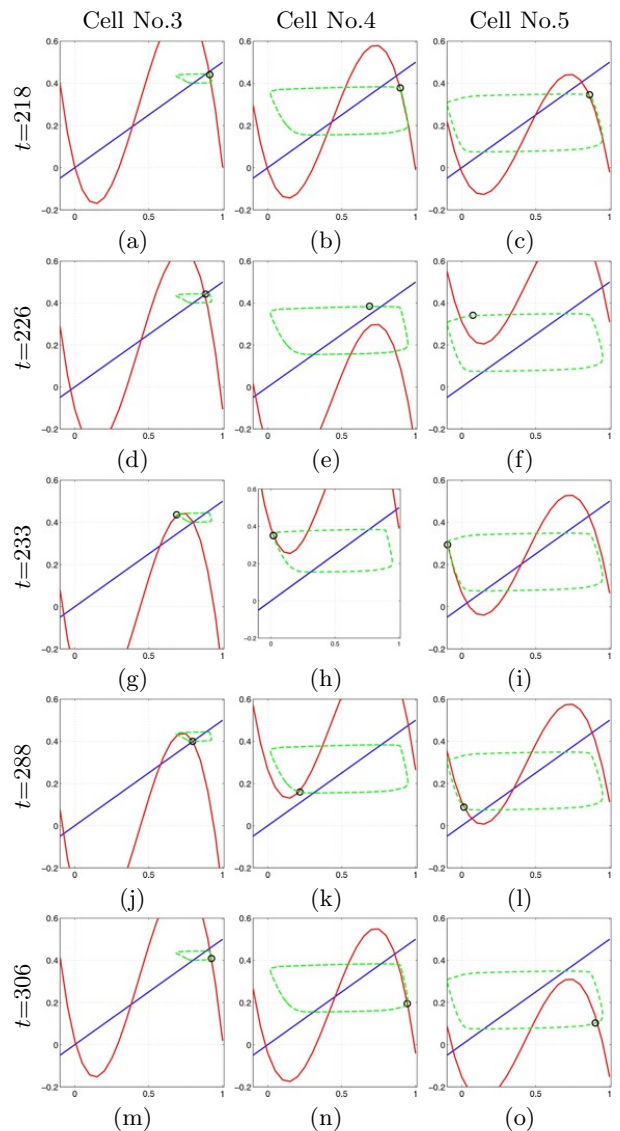


FIG. 11: Phase portrait diagrams with snapshots of the dynamical nullcline. Rows indicate the time evolution from the top down, and columns indicate the number of cells (3 at left, 4 at middle and 5 at right). Green dashed curves are the limit cycle solution. Red cubic function curves are the nullcline of $\dot{u}_i = 0$. Blue straight lines are the nullcline of $\dot{v}_i = 0$. Blue circles are the position of (u_i, v_i) at specific times.

$F(\cdot)$ dynamically moves up and down in the phase plane, corresponding to the state of u_{i-1}, u_i, u_{i+1} .

In Fig. 11, we show the phase portrait of cells around the oscillation border (cells No.3-5), as well as their dynamical nullcline at some turning points. Snapshots are taken under the same conditions of normal oscillation as shown in Fig. 3.

The first row, (a, b, c) of Fig. 11 are all in the excited state, i.e., for all three cells, u_i is close to 1. Therefore, under this condition, the vertical offset ΔU of the nullcline is nearly zero, and all three cells exhibit bistability. The second row is taken at $t = 226$, when

the wave back comes (see Fig. 4(d)), and the 3^{rd} cell moves towards its lower equilibrium (Fig. 11(f)). Since $\Delta U_4 = \tilde{D}(u_3 + u_5 - 2u_4)$, a sudden drop in u_5 leads to a rapid decrease in the cubic nullcline. As shown in Fig. 11(e), the red cubic nullcline moves down so that the higher equilibrium disappears. Thus, the 4^{th} cell becomes mono-stable and the state quickly converges to the left branch of the cubic nullcline. As time progresses, the decrease in u_4 makes the nullcline of the 3^{rd} cell move down. However, since the 3^{rd} cell has a larger Γ , which controls the amplitude of the cubic nullcline, even if u_4 decreases to its lowest value (Fig. 11(h)), i.e., ΔU_3 reduces to its minimum, the cubic and straight nullclines still intersect. This explains why the wave back passes the 4^{th} cell, but stops at the 3^{rd} cell (Fig. 4(a)). After propagation stops, there is a relatively long stationary period from time 230 to 300. In this interval, there is a slow decrease in the inhibitor v_4 . Since $u_3 \approx 1$ and $u_5 \approx 0$, ΔU_4 is so large that the cubic nullcline is above the straight nullcline (Fig. 11(k)). Under this condition, the cell is mono-stable, with the equilibrium at the right branch of the cubic function. Thus, after a while, the state of u will switch to a higher value (Fig. 11(n)), and leads to a reflecting wave (Fig. 4(f)). Note that a smaller coupling strength \tilde{D} leads to a smaller offset ΔU . If we move down the cubic nullcline slightly to cross the straight nullcline in Fig. 11(k), the 4^{th} cell becomes bistable. This will disable the switch from left to right, and stop the oscillation (Fig. 5).

From the above description and Fig. 11, we conclude that the boundary cell, which is bistable without coupling, turns to switch between two types of mono-stable dynamics. This switching becomes the power that underlies the self-sustained oscillation observed in the present model. The variation of the offset of the dynamical nullcline of the boundary cell gives rise to rich oscillation phenomena.

C. Conditions for oscillation

We will now explore the conditions for oscillation in an approximate manner by studying the dynamics on the oscillation border, where wave backs (WB) stop and wave fronts (WF) generate. Based on an investigation of the dynamical nullcline and state variable, we concluded that a wave back will not pass a critical cell, c , if the nullclines still intersect when cell $c + 1$ has dropped to its lower equilibrium (Fig. 11(g,h)). In contrast, if the intersections disappear, the state of u_c will switch to a lower equilibrium and cell c may oscillate (Fig. 11(e,f)). Similarly, to fire a wave front, the two nullclines of an edge cell can not cross when the state of the inhibitor recovers to its lower limit.

Thus, we can roughly solve the condition by finding two possible tangency for the two nullclines Eq. (10) and Eq. (11). This can be achieved using the following equa-

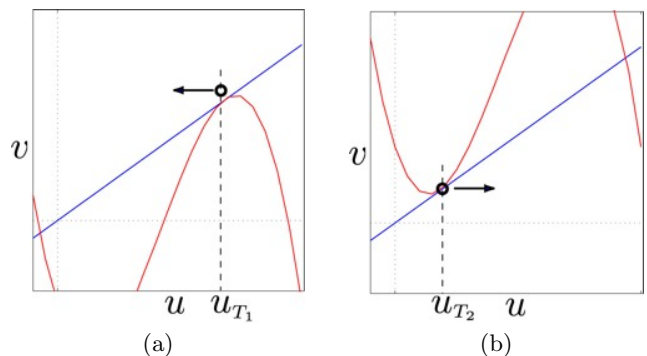


FIG. 12: Schematic diagram of two critical tangency situations, corresponding to the conditions for which (a) a wave back passes and (b) a wave front is generated. Black circles are the position of states when two nullclines tangent to each other.

tions:

$$\frac{dF(u, \Gamma)}{du} = \frac{dG(u)}{du}, \quad (12)$$

Equation (12) is for two nullclines with the same slope. By substituting F and G into Eq. (12), we have

$$\Gamma(-3u^2 + 2(1 + \alpha)u - \alpha) = \beta, \quad (13)$$

from which we obtain two solutions

$$u_{T_{1,2}} = \frac{13 \pm \sqrt{79 - 150/\Gamma}}{30}. \quad (14)$$

For cell c to propagate a wave back, there should be only a lower equilibrium when u_c close to the higher tangency point. The corresponding condition is $F(u_{T_1}, \Gamma_c) < G(u_{T_1})$. Substitution leads to

$$\Gamma_c u_{T_1} (u_{T_1} - \alpha)(1 - u_{T_1}) + \tilde{D}(u_{c-1} + u_{c+1} - 2u_{T_1}) < \beta u_{T_1}. \quad (15)$$

On the other hand, for cell c to generate a wave front, there should be no lower equilibrium when u_c is close to the lower tangency point. This simply means that $F(u_{T_2}, \Gamma_c) > G(u_{T_2})$, which can be rewritten as

$$\Gamma_c u_{T_2} (u_{T_2} - \alpha)(1 - u_{T_2}) + \tilde{D}(u_{c-1} + u_{c+1} - 2u_{T_2}) > \beta u_{T_2}. \quad (16)$$

Two critical conditions are shown in Fig. 12.

Approximation

1. u_{c-1} is the “distal” side of the critical cell c . It remains in its higher equilibrium since the wave back can not pass it. Thus, we can approximate it by finding the biggest intersection of the two nullclines. In the wave back case, since u_{T_1} is close to the higher equilibrium, ΔU_{c-1} is nearly zero. Thus, we determine u_{c-1} to be 0.9. In the wave front case, however, u_{T_2} is small. If we consider the minus ΔU_{c-1} , we determine u_{c-1} to be 0.8.

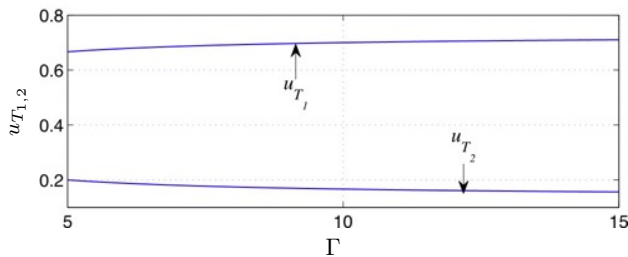


FIG. 13: Variation of two tangent points $u_{T_{1,2}}$ with respect to Γ .

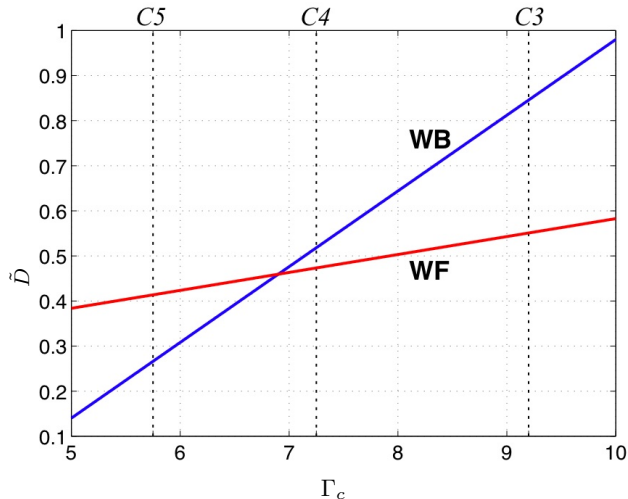


FIG. 14: The diagram in the parameter plan (Γ_c, \tilde{D}) representing the conditions of collective oscillation. A wave back passes the cell, and a wave front reflects, when the parameters are above the blue (WB) and red (WF) line, respectively.

2. u_{c+1} is the “proximal” side of the critical cell c . It switches off before cell c when a wave back comes and waits to be excited again by cell c , so at the critical time, u_{c+1} approaches 0.
3. Figure 13 shows $u_{T_{1,2}}$ according to Eq. (14). Obviously, u_{T_1} and u_{T_2} change little, and can be regarded as the constants 0.7 and 0.17, respectively.
4. Note that the above approximations are not valid when the coupling strength is too large.

According to the above approximations, by substituting

$$u_{T_1} = 0.7, u_{c-1} = 0.9, u_{c+1} = 0$$

into Eq. (15), and

$$u_{T_2} = 0.17, u_{c-1} = 0.8, u_{c+1} = 0$$

into Eq. (16), we obtain two rough conditions

$$0.084\Gamma_c - 0.5\tilde{D} < 0.35 \quad \text{WB passes,} \quad (17)$$

$$-0.0183\Gamma_c + 0.46\tilde{D} > 0.085 \quad \text{WF generates.} \quad (18)$$

Clearly, the critical coupling strength increases linearly with respect to the active factor Γ . We draw two lines in Fig. 14, where the blue (WB) and red (WF) lines are obtained from Eq. (17) and Eq. (18), respectively. In Fig. 14, C_3 , C_4 and C_5 on the top horizontal axis indicate the value of Γ defined by Eq. (4) for cells 3, 4 and 5, respectively. Lines WF and WB cross each other between C_4 and C_5 . This kind of topology makes the 4th and 5th cells behave completely different.

For cell 5, WF is above WB. If the coupling strength is between WF and WB, a wave back coming from the center can switch the 4th cell OFF, but the cell can not be switched ON to fire a wave front. This is exactly the situation shown in Fig. 5, in which no oscillation takes place. On the other hand, for cell 4, WF is below WB. Clearly, if the coupling strength allows the wave back to suppress the 4th cell, the cell will be excited again and lead to a wave front.

The conditions for these two situations depend on many other factors, such as the initial conditions, propagation velocity, cell excitability, and so on. The situation is much more complicated than the approximated case we have discussed here. Qualitatively, we can conclude that the intersection of these two condition lines is the origin of self-sustained collective oscillation.

V. CONCLUDING REMARKS

In this paper, we have proposed a new scenario for self-organized and self-sustained oscillation in multi-cellular biological tissue. In contrast to the usual framework based on an oscillatory genetic network, the present system does not include any self-oscillating cells. However, by coupling several cells together, we can observe collective oscillation inside a group of cells, i.e., tissue. Moreover, oscillation can manifest itself in several ways, corresponding to different coupling strengths. Anti-phase and in-phase oscillations at the two boundaries lead to changes in the position of oscillation and the oscillating cell population, respectively. The birth and death of oscillation resulting from variation in the coupling strength were also discussed. We also provide a general idea of how the size of the field in which cells grow affects the oscillatory behavior. It is of interest to extend our new hypothesis to spatial three dimensional systems, i.e., a more realistic model of living organism. Finally, a detailed investigation of the dynamical movement of the nullcline provided insight into the mechanism of complicated oscillatory phenomena. Although there have been several studies on self-oscillatory phenomena in spatially discrete systems in the context of mathematics and physics, this paper extends these basic ideas to spatio-temporal self-organization in a biological system.

Our observations were based on a numerical simulation. Future analytical studies inspired by these interesting phenomenon are needed. At last, but not less important, we are going to cooperate with biologists,

in order to design corresponding biological experiments and to explore more proofs supporting our hypothesis.

-
- [1] U. Schibler and F. Naef, *Current Opinion in Cell Biology* **17**, 223 (2005).
- [2] O. Pourquie, *Science* **301**, 328 (2003).
- [3] J. Stark, C. Chan, and A. J. T. George, *Immunological Reviews* **216**, 213 (2007).
- [4] G. Tiana, S. Krishna, S. Pigolotti, M. H. Jensen, and K. Sneppen, *Physical Biology* **4**, R1 (2007).
- [5] H. Hirata, S. Yoshiura, T. Ohtsuka, Y. Bessho, T. Harada, K. Yoshikawa, and R. Kageyama, *Science* **298**, 840 (2002).
- [6] A. Hoffmann, A. Levchenko, M. L. Scott, and D. Baltimore, *Science* **298**, 1241 (2002).
- [7] J. Lewis, *Current Biology* **13**, 1398 (2003).
- [8] L. Chen and K. Aihara, *Circuits and Systems I, IEEE Transactions on* **49**, 1429 (2002).
- [9] Y. Masamizu, T. Ohtsuka, Y. Takashima, H. Nagahara, Y. Takenaka, K. Yoshikawa, H. Okamura, and R. Kageyama, *PNAS* **103**, 1313 (2006).
- [10] D. Gonze and A. Goldbeter, *Chaos* **16**, 026110 (2006).
- [11] J. Garcia-Ojalvo, M. Elowitz, and S. Strogatz, *PNAS* **101**, 10955 (2004).
- [12] M. Pérez-Armendariz, C. Roy, D. C. Spray, and M. V. Bennett, *Biophysical Journal* **59**, 76 (1991).
- [13] R. Bertram and A. Sherman, *J Biosci* **25**, 197 (2000).
- [14] J. S. O'Neill, E. S. Maywood, J. E. Chesham, J. S. Takahashi, and M. H. Hastings, *Science* **320**, 949 (2008).
- [15] T. Yanagita, Y. Nishiura, and R. Kobayashi, *Physical Review E* **71**, 036226 (2005).
- [16] O. Nekhamkina and M. Sheintuch, *Physical Review E* **73**, 066224 (2006).
- [17] J. H. Cartwright, *Physical review E* **62**, 1149 (2000).
- [18] S. Smale, in *The Hopf Bifurcation and Its Application*, edited by J. E. Marsden and M. McCracken (Springer-Verlag, NY, 1974), chap. 11.
- [19] A. Y. Pogromsky, *International Journal of Bifurcation and Chaos* **8**, 295 (1998).
- [20] A. Pogromsky, T. Glad, and H. Nijmeijer, *International Journal of Bifurcation and Chaos* pp. 629–644 (1999).
- [21] A. Gomez-Marin, J. Garcia-Ojalvo, and J. M. Sancho, *Physical Review Letters* **98**, 168303 (2007).
- [22] P. Couillet, J. Lega, B. Houchmanzadeh, and J. Lajzerowicz, *Physical Review Letters* **65**, 1352 (1990).
- [23] A. Hagberg and E. Meron, *Chaos* **4**, 477 (1994).
- [24] M. Bode, *Physica D: Nonlinear Phenomena* pp. 270–286 (1997).
- [25] A. Prat and Y. Li, *Physica D: Nonlinear Phenomena* pp. 50–68 (2003).
- [26] A. Prat, Y. Li, and P. Bressloff, *Physica D: Nonlinear Phenomena* pp. 177–199 (2005).
- [27] Y. Li, *Physica D: Nonlinear Phenomena* pp. 27–49 (2003).
- [28] J. Miyazaki and S. Kinoshita, *Physical Review E* **76**, 066201 (2007).
- [29] N. M. Shnerb, Y. Louzoun, E. Bettelheim, and S. Solomon, *PNAS* **97**, 10322 (2000).
- [30] J. P. Keener, *SIAM J. Appl. Math.* **47**, 556 (1987).
- [31] A. M. Turing, *Philos. Trans. R. Soc. London* **B327**, 37 (1952).
- [32] R. Kageyama, Y. Masamizu, and Y. Niwa, *Developmental Dynamics* **236**, 1403 (2007).
- [33] M. Ibanes and J. C. I. Belmonte, *Molecular Systems Biology* **4** (2008).
- [34] D. Ben-Zvi, B.-Z. Shilo, A. Fainsod, and N. Barkai, *Nature* **453**, 1205 (2008).
- [35] L. Wolpert, *J. Theoret. Biol.* **25**, 1 (1969).
- [36] P. Ashwin and M. Timme, *Nature* **436**, 36 (2005).
- [37] D. Angeli, J. James E. Ferrell, and E. D. Sontag, *PNAS* **101**, 1822 (2007).
- [38] J. M. A. M. Kusters, J. M. Cortes, W. P. M. van Meerwijk, D. L. Ypey, A. P. R. Theuvenet, and C. C. A. M. Gielen, *Physical Review Letters* **98**, 098107 (2007).
- [39] H. Maamar, A. Raj, and D. Dubnau, *Science* **317**, 526 (2007).
- [40] J.-R. Kim, Y. Yoon, and K.-H. Cho, *Biophysical Journal* **94**, 359 (2008).
- [41] L. J. Holt, A. N. Krutchinsky, and D. O. Morgan, *Nature* **454**, 353 (2008).
- [42] F. Luckel, K. Kubo, K. Tsumoto, and K. Yoshikawa, *FEBS Letters* **579**, 5119 (2005).
- [43] N. Makita and K. Yoshikawa, *FEBS Letters* **460**, 333 (1999).
- [44] K. Tsumoto and K. Yoshikawa, *Biophysical Chemistry* **82**, 1 (1999).
- [45] Y. S. Mamasakhlisov, S. Hayryan, V. F. Morozov, and C.-K. Hu, *Physical Review E* **75**, 061907 (2007).
- [46] P. Schanda, V. Forge, and B. Brutscher, *PNAS* **104**, 11257 (2007).
- [47] S. Etienne-Manneville and A. Hall, *Nature* **420**, 629 (2002).